JOURNAL OF PROPULSION AND POWER
Vol. 24, No. 4, July–August 2008

Computational Study on the Critical Nozzle Flow of High-Pressure Hydrogen Gas

Jae-hyung Kim* and Heuy-dong Kim†
Andong National University, Gyeongbuk 760-749, Republic of Korea
and
Toshiaki Setoguchi‡ and Sigeru Matsuo§
Saga University, Saga 840-8502, Japan

DOI: 10.2514/1.30976

The critical nozzle has frequently been employed to measure the flow rate of various gases, but hydrogen gas, especially at high-pressure conditions, was not dealt with nearly as much using the critical nozzle due to treatment danger. According to experimental data obtained recently, it was reported that the discharge coefficient of hydrogen gas through the critical nozzle exceeds unity in a specific range of Reynolds numbers. No detailed explanation on such an unreasonable value was made, but it was vaguely inferred as real gas effects. For the purpose of the practical use of high-pressure hydrogen gas, systematic research is required to clarify the critical nozzle flow of high-pressure hydrogen gas. In the present study, a computational fluid dynamics method has been applied to predict the critical nozzle flow of high-pressure hydrogen gas. Several kinds of real gas equations that take into account the forces and volume of molecules of hydrogen gas were incorporated into the axisymmetric, compressible Navier–Stokes equations. A fully implicit finite volume scheme was used to numerically solve the governing equations. The computational results were validated with available experimental data. The results show that the discharge coefficient is mainly influenced by the compressibility factor and the specific heat ratio, which appear more remarkable as the inlet total pressure of hydrogen gas increases.

Nomenclature

A^* = cross-sectional area at nozzle throat
C_d = discharge coefficient
C_p = specific heat at constant pressure
C^* = critical flow factor
c = speed of sound
D = diameter of nozzle throat
E = internal energy
H = total enthalpy per unit mass
K = thermal conductivity
M_w = molecular weight
$\dot{m}$ = mass flow rate
p_a = absolute pressure, back pressure
p_c = critical pressure
p_o = inlet total pressure
p_s = static pressure
R = gas constant
Re = Reynolds number
S = entropy
T = temperature
T_c = critical temperature
T_o = inlet total temperature
t = time
v = velocity
v_c = critical specific volume
x = distance
Z = compressibility factor
γ = specific heat ratio
μ = viscosity coefficient
ρ = density

Received 13 March 2007; accepted for publication 4 March 2008.

*Researcher, School of Mechanical Engineering, Andong; xflying@hanmail.net.
†Professor, School of Mechanical Engineering, Andong; kimhd@andong.ac.kr. Member AIAA.
‡Professor, Department of Mechanical Engineering, 1, Honjo-machi; setoguci@me.saga-u.ac.jp.
§Professor, Department of Mechanical Engineering, 1, Honjo-machi; matsuo@me.saga-u.ac.jp.

Introduction

THE critical nozzle is one of the flow metering devices being used extensively in industrial areas dealing with gases. It makes use of the concept of flow choke that occurs at the nozzle throat [1]. Under choked flow conditions, pressure variations in the flowfield downstream of the nozzle have a negligible influence on the mass flow rate, and the coefficient of discharge is easily obtained only by the flow properties measured upstream of the nozzle. According to one-dimensional gas dynamics theory, the mass flow through the critical nozzle is given as a function of the pressure and temperature upstream of the nozzle, the nozzle throat diameter, and the specific heat ratio of gas [2].

A considerable amount of research has investigated the gas flow features through the critical nozzle. According to these results [3–5], the mass flow rate and critical pressure ratio are strong functions of the Reynolds number, based upon the velocity at the nozzle throat and the diameter of nozzle throat. At high Reynolds numbers, the coefficient of discharge approaches unity, indicating that the one-dimensional, inviscid theory reasonably predicts the mass flow. It is known that at lower Reynolds numbers, the coefficient of discharge is considerably lower than unity [6,7]. This is due to the wall boundary-layer effects on the mass flow rate through the critical nozzle.

Recently, Kim et al. [8,9] reported the discharge coefficients of a variety of gases for a quite wide range of Reynolds numbers using a computational fluid dynamics method. The flow characteristics through the critical nozzle have been well documented at both considerably low and high Reynolds number regimes.

Of the many kinds of working gases employed in industrial field, hydrogen gas is one of the most promising gases as alternative energy for the future. For instance, a hydrogen fuel cell, which is being considered as the driving power system of vehicles, yields high-pressure hydrogen gas nearly at atmospheric temperature. In such an

application, precise measurement of the flow rate is of practical importance to the mileage and power output of the vehicle.

In the past, a large number of works [10–13] have investigated the thermophysical properties of hydrogen gas, which are specified by some different kinds of the equations of state, the critical pressure, the compressibility factor of hydrogen gas, etc.

However, to date, only a few studies have focused on the mass flow rate of high-pressure hydrogen gas through the critical nozzle, due to treatment difficulties. Recently, Nakao [14] conducted the flow rate measurement of hydrogen gas using a critical nozzle and found that the discharge coefficient of hydrogen gas exceeds unity in a specific Reynolds number regime. He vaguely inferred that this unreasonable value of the discharge coefficient would be due to real gas effects or any other measurement errors. No detailed explanation has been made for this abnormal discharge coefficient of high-pressure hydrogen gas.

Some researchers [5,8,9] are devoted to computations of the axisymmetric Navier–Stokes equations, but they have employed the perfect gas law to simulate the critical nozzle flows. Therefore, all of the research conducted has failed in predicting such unreasonable behavior of the discharge coefficient at high-pressure conditions. To the authors' knowledge, there is no work documenting the real gas effects on the critical nozzle flows at high-pressure conditions. The present study aims at investigating the detailed flow of high-pressure hydrogen gas through the critical nozzle, with the help of a computational fluid dynamics (CFD) method. In the computations, several kinds of real gas equations that take into account the forces and volume effects of the intermolecules of hydrogen gas were incorporated into the axisymmetric, compressible Navier–Stokes equations. A fully implicit finite volume scheme was used to numerically solve the governing equations. The computational results were validated with available experimental data.

Computational Analysis

Governing Equations

The high-pressure hydrogen gas flow through the critical nozzle is simulated using a CFD method. The governing equations are given by the conservation forms of mass, momentum, and energy. The axisymmetric, mass averaged, time-dependent Navier–Stokes equations, which use a k–ε turbulent model, are employed in the present computations [1,8]. The resulting equations are expressed in an integral form:

$$\Gamma \frac{\partial}{\partial t} \int_V Q \, \mathrm{d}V + \oint [F - G] \, \mathrm{d}A = 0 \tag{1}$$

where F and G are the inviscid and viscous flux vectors in the standard conservation form and Q is the dependent vector of the primary variables.

$$\begin{aligned} F &= [\rho v, \rho v v_x + p\hat{i}, \rho v v_y + p\hat{j}, \rho v v_z + p\hat{k}, \rho v H]^T \\ G &= [0, \tau_{xi}, \tau_{ji}, \tau_{zi}, \tau_{ij} v_j + q]^T \qquad Q = [p, v_x, v_y, v_z, T]^T \end{aligned} \tag{2}$$

In these equations, H is the total enthalpy per unit mass and is related to the total energy E by $H = E + p/\rho$, where E includes both internal and kinetic energies. The preconditioning matrix Γ is included in Eq. (1) to provide an efficient solution of the present axisymmetric compressible flow. This matrix is given by

$$\Gamma = \begin{bmatrix} \theta & 0 & 0 & 0 & \rho_T \\ \theta v_x & \rho & 0 & 0 & \rho_T v_x \\ \theta v_y & 0 & \rho & 0 & \rho_T v_y \\ \theta v_z & 0 & 0 & \rho & \rho_T v_z \\ \theta H & \rho v_x & \rho v_y & \rho v_z & \rho_T H + \rho C_p \end{bmatrix} \tag{3}$$

where ρ_T is the derivative of the density with respect to the temperature at a constant pressure. The parameter θ is defined as

$$\theta = (1/U_r^2) - (\rho_T H + \rho C_p) \tag{4}$$

In Eq. (4), the reference velocity U_r is chosen such that the eigenvalues of the system remain well conditioned with respect to the convective and diffusive time scales, and C_p is the specific heat at a constant pressure.

The preconditioned governing equations are discretized spatially using a finite volume scheme in which the physical domain is subdivided into numerical cells and the integral equations are applied to each cell. Also, for the time derivatives in the governing equations, an implicit multistage time stepping scheme, which is advanced from time t to time $t + \Delta t$ with a multistage Runge–Kutta scheme, is used.

Equations of State of Real Gas

Hydrogen gas has little attraction between molecules so that it is inert in character until the molecules are disrupted. Major properties of such a hydrogen gas are summarized in Table 1. The critical temperature and pressure are −240°C (33 K) and 1.3 MPa, respectively. Assuming an ideal gas, the specific heat ratio of hydrogen gas is about 1.41.

Many works have been conducted to document these thermodynamic properties of hydrogen gas, which are in a thermodynamically equilibrium state or in low-speed flows with negligible compressibility effects. However, the critical nozzle flows are transonic or supersonic, being subject to strong compressibility effects. The real gas effects of hydrogen gas at high-pressure conditions should be fully incorporated into the governing equation system.

Meanwhile, the compressibility factor (Z) has been often used to evaluate the real gas effects, as

$$Z = \frac{pv}{RT} \tag{5}$$

According to Eq. (5), the compressibility factor of real gas is influenced by both the temperature and pressure and is expressed by a form of power series using virial coefficients. From the point of view of kinetic theory or statistical thermodynamics of hydrogen gas, Eq. (6), called a virial equation, is frequently given as a polynomial function of specific volume:

$$Z = \frac{pv}{RT} = 1 + \frac{B(T)}{v} + \frac{C(T)}{v^2} + \frac{D(T)}{v^3} + \cdots \tag{6}$$

where $B(T)$, $C(T)$, and $D(T)$ are the virial coefficients that are dependent only on temperature.

Equation (6) can be used to document the p–v–T behaviors for all gases, but it is often troublesome due to the infinite series. Some cubic equations of state using a molecular volume are alternatively employed to explain the p–v–T behaviors in a wide range of temperatures and pressures, which are based upon van der Waals equation and the Benedict–Webb–Rubin (BWR) equation [15]. Later, in Yang et al. [16], Lee and Kesler modified the BWR equation as follows:

$$Z = \frac{p_r v_r'}{T_r} = 1 + \frac{B}{v_r'} + \frac{C}{v_r'^2} + \frac{D}{v_r'^5} + \frac{c_4}{T_r^3 v_r'^2}\left(\beta + \frac{\gamma}{v_r'^2}\right) \exp\left(-\frac{\gamma}{v_r'^2}\right) \tag{7}$$

where p_r, T_r, and v_r are the reduced pressure, temperature, and specific volume, respectively, based on the critical point, which is denoted by the subscript c, and these are defined as

Table 1 Thermodynamic properties of hydrogen gas

Gas constant	Specific heat ratio	Critical pressure	Critical temperature	Critical compressibility factor	Molecular weight
4120 J/kg · K	1.41	1.3 MPa	33.3 K	0.306	2.016 kg/kmol

$$p_r = \frac{p}{p_c}, \qquad T_r = \frac{T}{T_c}, \qquad v_r = \frac{v}{v_c} \tag{8}$$

In Eq. (3), B, C, and D are given by

$$B = b_1 - \frac{b_2}{T_r} - \frac{b_3}{T_r^2} - \frac{b_4}{T_r^3}, \qquad C = c_1 - \frac{c_2}{T_r} + \frac{c_3}{T_r^3},$$
$$D = d_1 + \frac{d_2}{T_r}$$

The variable v_r' is defined as

$$v_r' = \frac{v}{RT_c/p_c} \tag{9}$$

where v_r' is equally treated with the reduced specific volume ($v_r = v/v_c$) in Eq. (8).

Redlich and Kwong have improved the van der Waals equation to obtain the compressibility factor more accurately, as follows [12]:

$$p = \frac{RT}{v - \tilde{b}} - \frac{a(T)}{v(v + b_0)} \tag{10}$$

where

$$v = \frac{1}{\rho}, \qquad a(T) = a_0\left(\frac{T_c}{T}\right)^n, \qquad \tilde{b} = b_0 - c$$
$$a_0 = 0.42747\frac{R^2T_c^2}{p_c}, \qquad b_0 = 0.08664\frac{RT_c}{p_c},$$
$$c_0 = \frac{RT_c}{p_c + \frac{a_0}{v_c(v_c + b_0)}} + b_0 - v$$

In the case of hydrogen gas, the n value in the function of $a(T)$ is given by $n = 0.31$. In general, Eq. (10) can be expressed as a polynomial function of the specific volume:

$$v^3 + a_1v^2 + a_2v + a_3 = 0 \tag{11}$$

where

$$a_1 = c_0 - \frac{RT}{p}, \qquad a_2 = -\left(\tilde{b}b_0 + \frac{RTb_0}{p} - \frac{a(T)}{p}\right),$$
$$a_3 = -\frac{a(T)\tilde{b}}{p}$$

The derivatives of the specific volume with respect to the temperature and pressure can be determined from Eq. (10) using implicit differentiation:

$$\left(\frac{\partial v}{\partial p}\right)_T = -\frac{(a_1)_p'v^2 + (a_2)_p'v + (a_3)_p'}{3v^2 + 2a_1v + a_2} \tag{12}$$

$$\left(\frac{\partial v}{\partial T}\right)_p = -\frac{(a_1)_T'v^2 + (a_2)_T'v + (a_3)_T'}{3v^2 + 2a_1v + a_2} \tag{13}$$

$$(a_1)_p' = \frac{RT}{p^2}, \qquad (a_2)_p' = \frac{RTb_0 - a(T)}{p^2}, \qquad (a_3)_p' = \frac{a(T)\tilde{b}}{p^2}$$
$$(a_1)_T' = -\frac{R}{p}, \qquad (a_2)_T' = \frac{-Rb_0 + \frac{da(T)}{dT}}{p},$$
$$(a_3)_T' = -\frac{\mathrm{d}a(T)}{\mathrm{d}T}\frac{\tilde{b}}{p}, \qquad \frac{\mathrm{d}a(T)}{\mathrm{d}T} = -n\frac{a(T)}{T}$$

Using Eqs. (12) and (13), the derivatives of density can be obtained from the following relations:

$$\left(\frac{\partial \rho}{\partial p}\right)_T = -\rho^2\left(\frac{\partial v}{\partial p}\right)_T \tag{14}$$

$$\left(\frac{\partial \rho}{\partial T}\right)_p = -\rho^2\left(\frac{\partial v}{\partial T}\right)_p \tag{15}$$

According to Augnier's work [17], the enthalpy of a real gas is given as

$$H = H^0(T) + pv - RT - \frac{a(T)}{b_0}(1 + n)\,\ell_n\left(\frac{v + b_0}{v}\right) \tag{16}$$

where $H^0(T)$ is the enthalpy function of a thermally perfect gas. In the present study, the specific heat of such a thermally perfect gas is assumed as

$$H^0(T) = \int_{T^0}^{T} C_p^0(T)\,\mathrm{d}T = C_1T + \frac{1}{2}C_2T^2 + \frac{1}{3}C_3T^3 + \frac{1}{4}C_4T^4$$
$$+ \frac{1}{5}C_5T^5 - H^0(T^0) \tag{17}$$

where C_1–C_5 are the polynomial coefficients, which are given by

$$C_1 = 12607.068, \qquad C_2 = 11.039948,$$
$$C_3 = -2.396044E - 2, \qquad C_4 = 2.2768604E - 5,$$
$$C_5 = -7.472688E - 9$$

Thus, the specific heat of a real gas can be obtained by differentiating Eq. (17) with respect to temperature:

$$C_p = \left(\frac{\partial H}{\partial T}\right)_p = C_p^0(T) + p\left(\frac{\partial v}{\partial T}\right)_p - R$$
$$- \frac{\mathrm{d}a(T)}{\mathrm{d}T}\frac{(1 + n)}{b_0}\,\ell_n\left(\frac{v + b_0}{v}\right) + a(T)(1 + n)\frac{\left(\frac{\partial v}{\partial T}\right)_p}{v(v + b_0)} \tag{18}$$

The derivative of the enthalpy with respect to the pressure is obtained using the following relation:

$$\left(\frac{\partial H}{\partial p}\right)_T = v - T\left(\frac{\partial v}{\partial T}\right)_p \tag{19}$$

where the entropy is given by

$$S = S^0(T, p^0) + R\,\ell_n\left(\frac{v - \tilde{b}}{v^0}\right) + \frac{\left(\frac{\mathrm{d}a(T)}{\mathrm{d}T}\right)}{b_0}\ell_n\left(\frac{v + b_0}{v}\right) \tag{20}$$

where the superscript 0 refers to a reference state based upon the ideal gas law. For an ideal gas at a fixed reference pressure p^0, the entropy is given by

$$S^0(T, p^0) = S(T^0, p^0) + \int_{T^0}^{T}\frac{C_p^0(T)}{T}\,\mathrm{d}T$$
$$= S(T^0, p^0) + C_1\,\ell_n(T) + C_2T + \frac{1}{2}C_3T^2 + \frac{1}{3}C_4T^3$$
$$+ \frac{1}{4}C_5T^4 - f(T^0) \tag{21}$$

The speed of sound of real gas is determined from the following thermodynamic relation:

$$c = v\sqrt{\left(\frac{C_p}{R - C_p}\right)\frac{1}{\left(\frac{\partial v}{\partial p}\right)_T}} \tag{22}$$

The dynamic viscosity is given as [18]

$$\mu(T) = 6.3 \times 10^{-7}\frac{M_w^{0.5}\,p_c^{0.6666}}{T_c^{0.1666}}\left(\frac{T_r^{1.5}}{T_r + 0.8}\right) \tag{23}$$

where T_r is the reduced temperature defined in Eq. (8) and M_w is the molecular weight of real gas.

Using this viscosity, the thermal conductivity is obtained from the Eucken formula [19]:

$$\kappa = \mu\left(C_P + \tfrac{5}{4}R\right) \tag{24}$$

In the present study, the thermodynamic properties obtained by these equations are incorporated into the governing equation system and numerically solved to assess the real gas effects of high-pressure hydrogen gas.

Figure 1 shows the effects of temperature and pressure on the compressibility factor Z of hydrogen gas. If hydrogen is assumed to be an ideal gas, the compressibility factor is 1.0, regardless of pressure. It is interesting to note that, in the cases of temperatures of 200 and 300 K, the virial equation of state predicts a monotonous increase in Z with pressure, whereas at a temperature of 100 K, it drops below 1.0 in the range of a certain pressure. Redlich–Kwong's equation of state gives similar results with the virial equation of state, whereas Lee–Kesler's equation of state predicts a little lower compressibility factor compared with the virial and the Redlich–Kwong's equations of state. It is known that the real gas effects differ depending on the equations of state employed. Thus, more systematic study is required to accurately evaluate the hydrogen gas flow at a high pressure. In the present study, Redlich–Kwong's equation of state is selected to simulate the high-pressure hydrogen gas through the critical nozzle, because it exhibits better agreement with the virial equation of state.

To scrutinize the dependence of the temperature and pressure on the compressibility factor of hydrogen gas, Fig. 2 shows the calculation results using Redlich–Kwong's equation of state. When the pressure is quite low, the compressibility factor approaches 1.0, the same as that of an ideal gas regardless of the temperature. However, as the pressure increases, the compressibility factor becomes a strong function of the temperature; at a low temperature, the compressibility factor decreases and then increases with pressure,

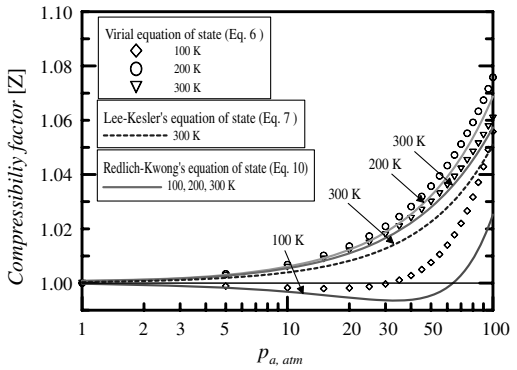

Fig. 1 Comparison of the equations of state of real gas.

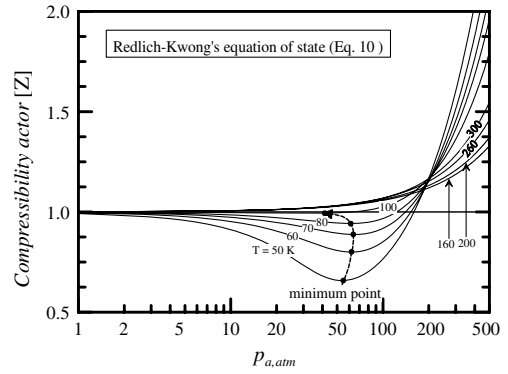

Fig. 2 Dependence of pressure on the compressibility factor of hydrogen gas.

after reaching a minimum value. It seems that the minimum value is dependent on the gas temperature. However, at a high temperature, such a trend is no longer found, and the compressibility factor is a simply increasing function of the pressure. This is because the molecular weight of hydrogen gas is very low and the intermolecular attraction force is less compared with the other gases.

Computational Conditions and Boundary Conditions

The critical nozzle employed in the present study is of a typical conical type [1,8] and its diameter D at the throat is 0.6 mm. A convergent part with a radius of curvature of $2.0D$ is given upstream of the nozzle throat. The straight divergent part has a half-angle of 4 deg, and its axial length is $5.0D$.

The computational domain and boundary conditions used in the present study are illustrated in Fig. 3. The pressure inlet and outlet boundary conditions are applied to the nozzle entrance and exit, respectively, where the inlet total pressure (p_o) and back pressure (p_a) of nozzle, respectively, are assumed. The symmetric conditions are assumed at the axis of the present critical nozzle, and this reduces a computational effort for the full domain. The adiabatic, no-slip condition is applied to the solid walls.

In the present study, the nozzle pressure ratio is defined as p_a/p_o and its value is constant at 0.5, but the inlet total pressure is varied in the range of 2.0–350.0 bar at a fixed total temperature, $T_0 = 288$ K.

Figure 4 shows the computational grid system. A structured grid system with about 45,000 grid points was employed in the present computations. The grids were densely clustered in the boundary layers and the nozzle throat so as to provide reasonable solutions. Several preliminary computations have been performed to ensure the grid independent solutions, using the available existing experimental data. The results have shown that the solutions obtained are no longer changed for more than 40,000 grid meshes.

Results and Discussion

In Fig. 5, the present computations are validated with the experimental results [20] using hydrogen and oxygen gases, in which the Reynolds number is based on the diameter of the nozzle throat and the total properties at the inlet of the nozzle. It is known that the coefficient of discharge is a strong function of the Reynolds number, and the predicted coefficients of discharge are in good agreement with the experimental results. It is believed that the present computational method effectively predicts the gas flow through the critical nozzle.

Figures 6 and 7 show the static pressure (p_s) distributions of the hydrogen gas flow along the nozzle axis and wall surface, respectively. The pressure ratio (p_a/p_o) is fixed at 0.5, and the axial distance (x) from the nozzle throat is normalized by the throat diameter (D). The static pressure along the nozzle axis decreases with the distance and then suddenly increases when the flow meets the shock wave, which has complicated structures due to the shock wave

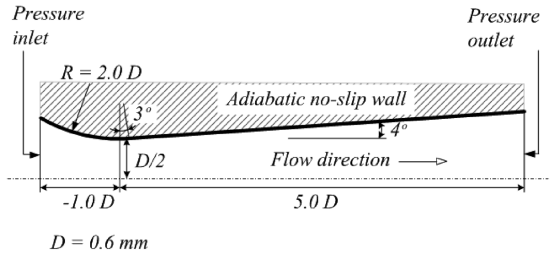

Fig. 3 Schematic diagram of the critical nozzle flowfield.

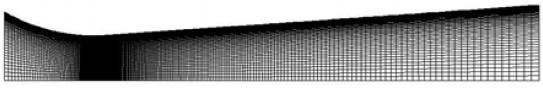

Fig. 4 Typical grid system.

boundary-layer interaction. The shock wave moves downstream as the inlet total pressure increases. It is noted that for the same p_o, the real gas effect causes the shock wave to be located further downstream compared with the ideal gas. This is qualitatively the same influence as the inlet total pressure on the shock locations.

Similar characteristics are also found in the static pressure distributions on the upper wall of the critical nozzle in Fig. 7, in which the static pressure rise at the shock waves is more gradual than that along the nozzle axis and the pressure jump is less, due to the stronger interaction between the shock wave and wall boundary layer. In both Figs. 6 and 7, it should be noted that the real gas effect reduces the static pressure at the nozzle throat compared with the ideal gas. This implies that the mass flow through the critical nozzle can be different due to the real gas effect.

Figure 8 shows the real gas effect on the mass flux at the nozzle throat. Note that ρu_{theo} means a theoretical mass flux at the throat, based upon the one-dimensional isentropic relation. At $p_o = 2.02$ MPa, the mass flux distributions for both the real and ideal gases are nearly the same, but at $p_o = 20.27$ MPa, they are different, mainly in the region outside the boundary layer.

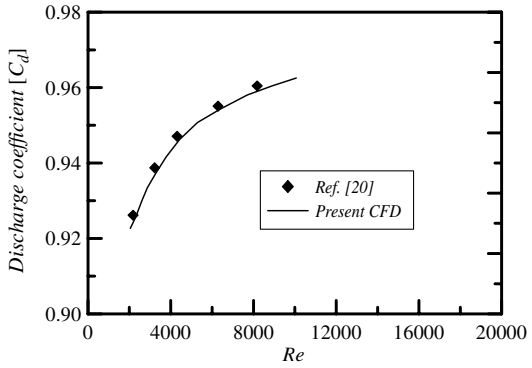

a) Hydrogen gas (H_2)

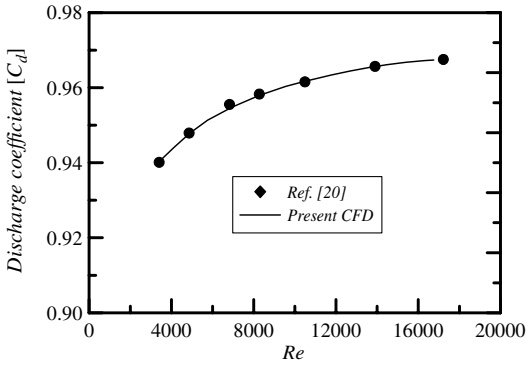

b) Oxygen gas (O_2)

Fig. 5 Comparison of the predicted and experimental discharge coefficients.

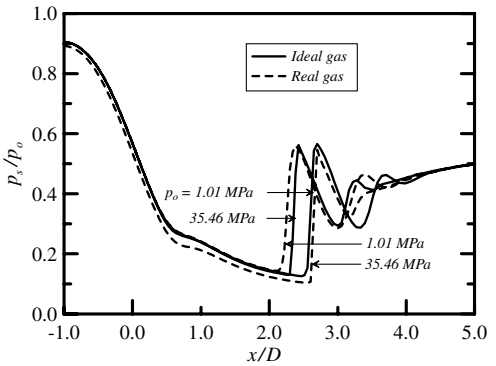

Fig. 6 Predicted static pressure distributions along the nozzle axis.

Meanwhile, according to the one-dimensional gas-dynamics theory, the theoretical mass flow rate through the critical nozzle is given by Eq. (25):

$$\dot{m} = A^* C^* p_o \sqrt{RT_o} \tag{25}$$

where A^* is the cross-sectional area at the nozzle throat and C^* is a critical flow factor, which is only defined in terms of the specific heat ratio:

$$C^* = \sqrt{\gamma} \times \left(\frac{\gamma+1}{2}\right)^{(1+\gamma/2(1-\gamma))} \tag{26}$$

The coefficient of the discharge C_d is usually defined as

$$C_d = \frac{\dot{m}}{\dot{m}_{\text{theo}}} \tag{27}$$

where $\dot{m}_{\text{theo}}$ is the mass flow rate calculated by the one-dimensional gas-dynamics theory.

Figure 9 shows the comparison of the predicted and experimental [14] discharge coefficients. At present, the only experimental data for high-pressure hydrogen gas are available in Nakao [14]. In 1965, Johnson [10] calculated the specific heat ratio using the virial equation of state and tabulated the thermodynamic properties of the hydrogen gas flow through the critical nozzle. These data are yielded in Eqs. (26) and (27) to obtain the coefficient of the discharge. It is interesting to note that the experimental data show a higher coefficient of the discharge than unity in the range of Reynolds number below 6.0×10^5. In the present study, this unreasonable trend, whether it comes from the real gas effect or from the experimental error, is not well understood.

One more noticeable trend in the coefficient of the discharge can be found in the range of Reynolds numbers above 6.0×10^5, where the coefficient of the discharge decreases with an increase in the Reynolds number. This obviously differs from the trend that has reported by many researchers [6–8]. A similar trend is found in

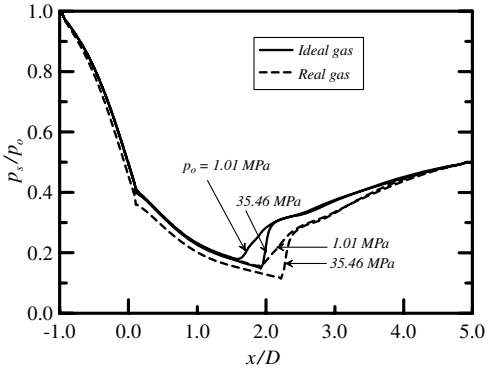

Fig. 7 Predicted static pressure distributions along the nozzle upper wall.

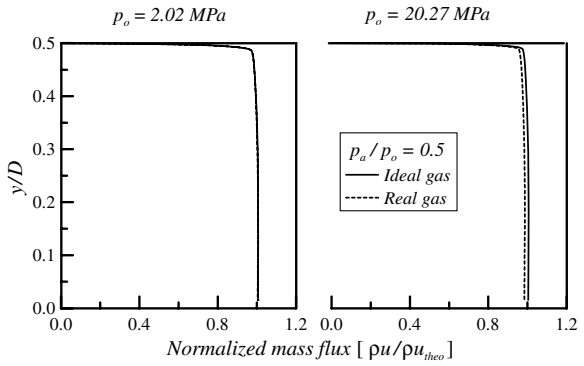

Fig. 8 Predicted mass flux profiles at the nozzle throat.

Johnson's data [10], but no data of the coefficient of the discharge exceed unity.

For an ideal gas assumption, the present computational results predict the coefficient of the discharge, which increases with the Reynolds number and then approaches a certain constant value [1]. However, the present computation taking into account the real gas effect is qualitatively similar to Johnson [10] and Nakao [14], but still fails in predicting the higher coefficient of the discharge than unity. Unfortunately, a clear and persuasive reasoning for this is, at present, not known. Such a trend in the discharge coefficient can give rise to a significant error in the mass flow of hydrogen gas at high-pressure conditions. More studies are needed to elucidate this ambiguous problem.

Figure 10 shows the real gas effect on the boundary-layer flow at the nozzle throat. It is known that the boundary-layer flow exhibits a typical turbulent profile expressed by the law of the wall and the law of the wake, in which the viscous sublayer occurs in the y^+ value less than 5.0. It seems that the boundary-layer profile becomes slightly fuller as p_o increases. It is, however, not obvious whether there is the real gas effect in the boundary-layer flow. Thus, it is believed that the variation in the C_d value with the Reynolds number does not stem from the displacement effect of the boundary-layer flow at the nozzle throat.

To investigate the real gas effect of hydrogen gas flow in more detail, the predicted compressibility factor and mass flux along the nozzle axis are presented in Figs. 11 and 12, together with the computed isodensity contours. For $p_o = 2.02$ MPa, some difference between the real and ideal gases is observed in the isodensity contours, mainly in the region downstream of $x/D = 2.0$. This is also found in the distributions of the mass flux along the nozzle axis, where both the cases are essentially the same upstream of the sudden jump that is generated by the shock wave, but the real gas effect causes the location of the sudden jump in the mass flux to move further downstream compared with the ideal gas.

The computed compressibility factors for the real gas seem to decrease during the acceleration of the flow through the nozzle throat and then slightly increase as it meets the shock wave. However, the computed compressibility factors for the real gas are slightly different from those of the ideal gas assumption, which are 1.0.

A big difference between the computed compressibility factors for the real and ideal gases can be found in Fig. 12, where $p_o = 20.27$ MPa. Upstream of the shock wave, at $x/D = 2.6$, the compressibility factor greatly decreases with the distance and, at the shock wave location, it sharply increases due to the compression effect of the shock wave. There is also some difference in the mass flux distributions upstream of the shock wave. Thus, it is concluded that at high-pressure conditions, the compressibility factor of the real gas can be one of the reasons for a variation of the discharge coefficients that were discussed in Fig. 9.

One of the flow properties influencing the mass flow rate of the real gas can be the specific heat ratio. Figure 13 shows the axial distributions of the computed values of the specific heat ratio of

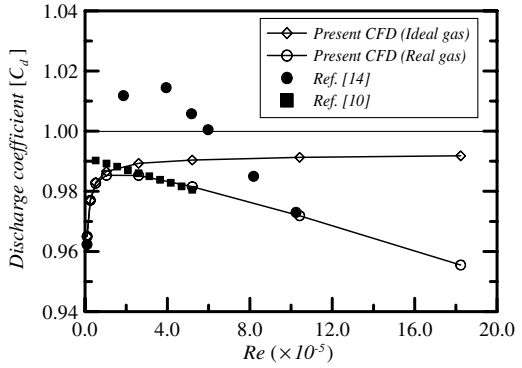

Fig. 9 Variation of the predicted and experimental discharge coefficients with Reynolds number.

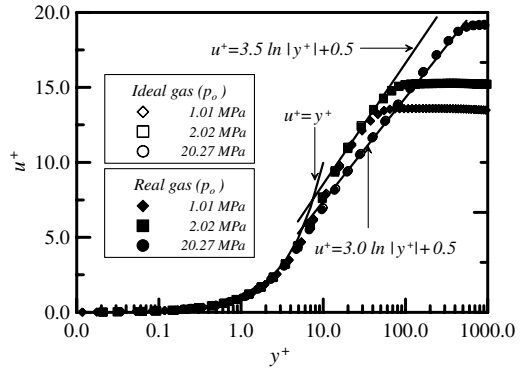

Fig. 10 Comparison of the boundary layer profiles at the nozzle throat.

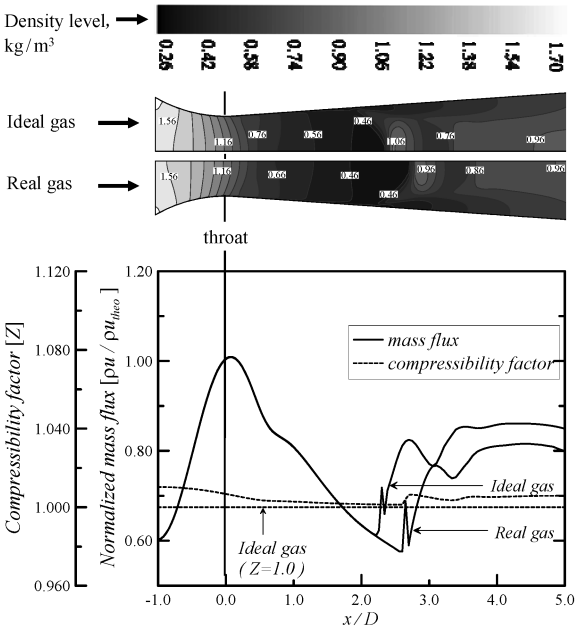

Fig. 11 Distributions of predicted compressibility factors and mass fluxes along the nozzle axis ($p_o = 2.02$ MPa).

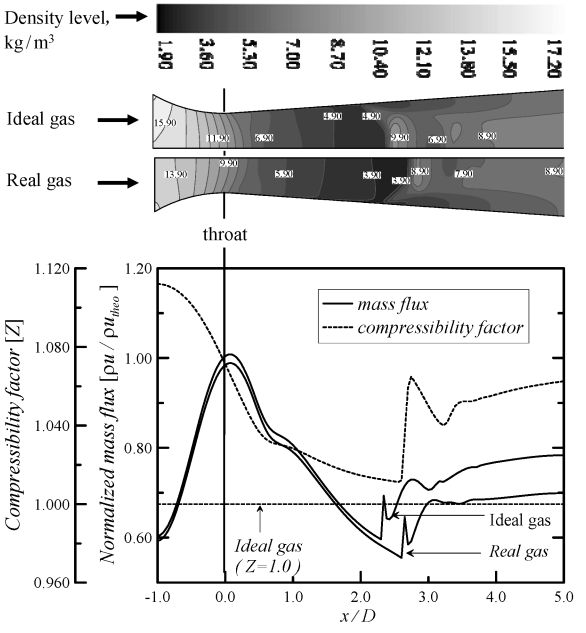

Fig. 12 Distributions of predicted compressibility factors and mass fluxes along the nozzle axis ($p_o = 20.27$ MPa).

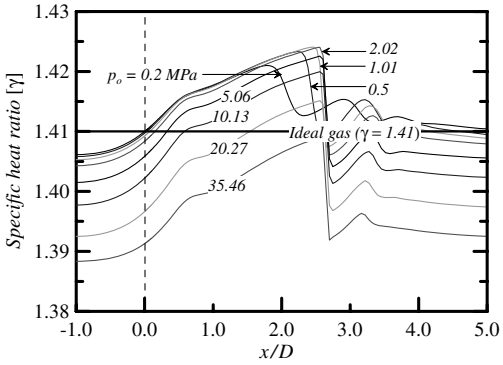

Fig. 13 Influence of the inlet total pressure on the specific heat ratio of hydrogen gas.

hydrogen gas. Note that the specific heat ratio for ideal gas is constant at 1.41. The specific heat ratio for real gas increases as the flow is accelerated through the nozzle throat, and it sharply decreases at the location of the shock wave. Such a tendency appears similarly for real gas, regardless of the p_o values applied. However, the sudden drop in the specific heats seems to be more significant when p_o increases. It is interesting to note that, at the nozzle throat, the specific heat ratio remains nearly constant at 1.41 when p_o is less then 1.01 MPa, but it significantly decreases as p_o increases. At the nozzle throat, this variation in the specific heat ratio with p_o has an appreciable importance on the mass flow rate of hydrogen gas through the critical nozzle. Therefore, the real gas effect should be included in evaluating the performance and accuracy of the critical nozzle as a flow metering device.

Conclusions

The present paper addresses a computational study to investigate the flow features of high-pressure hydrogen gas through the critical nozzle using a fully implicit finite volume method. To simulate the forces and volume effects of the intermolecules of hydrogen gas at a high pressure, several kinds of virial equations of state were employed and incorporated into the axisymmetric, compressible Navier–Stokes equations. The computational results were in good agreement with the critical nozzle flow with a comparatively low-pressure hydrogen gas, making them reasonably applicable to the ideal gas assumption, but they were not successful in accurately predicting the real gas effect at high-pressure conditions. The present study is the first attempt to simulate high-pressure hydrogen gas flow through the critical nozzle using a computational method, and it emphasizes the necessity of more research to properly predict the real gas effects occurring at high-pressure conditions.

Several important and meaningful conclusions obtained from the present study are summarized. Redlich-Kwong's equation of state predicts the real gas effects of high-pressure hydrogen gas comparatively well. However, unlike the coefficient of the discharge of ideal gas that has been obtained to date, the coefficient of the discharge of real gas through the critical nozzle decreases with an increase in the Reynolds number, as the Reynolds number exceeds a certain value. It is believed that this is not due to the displacement effect of the boundary layer at the nozzle throat but mainly results from the thermodynamic properties of real gas, such as the compressibility factor and the specific heat ratio, which appear more remarkable as the total pressure of hydrogen gas increases. Thus, the performance of the critical nozzle to measure high-pressure hydrogen gas flow should be studied and validated more systematically and thoroughly before practical application. In addition, more works should be directed to the improvement of the existing thermodynamic state of equations, which are reasonably capable of predicting the real gas effects in transonic and supersonic flows.

References

[1] Kim, H. D., Kim, J. H., Park, K. A., Setoguchi, T., and Matsuo, S., "Computational Study of the Gas Flow Through a Critical Nozzle," *Journal of Mechanical Engineering Science*, Vol. 217, No. 10, Oct. 2003, pp. 1179–1189.

[2] Tang, S. P., and Fenn, J. B., "Experimental Determination of the Discharge Coefficients for Critical Flow Through an Axisymmetric Nozzle," *AIAA Journal*, Vol. 16, No. 1, 1978, pp. 41–46. doi:10.2514/3.60854

[3] Arnberg, B. T., Britton, C. L., and Seidel, W. F., "Discharge Coefficient Correlations for Circular Arc Venturi Flow Meters at Critical (Sonic) Flow," *Journal of Fluids Engineering*, 1974, pp. 111–123.

[4] Kim, H. D., Kim, J. H., and Park, K. A., "Study for the Gas Flow Through a Critical Nozzle," American Society of Mechanical Engineers Paper 2003-45593, 2003.

[5] Kim, J. H., Kim, H. D., and Park, K. A., "Computational/Experimental Study of a Variable Critical Nozzle Flow," *Flow Measurement and Instrumentation*, Vol. 17, No. 2, 2006, pp. 81–86. doi:10.1016/j.flowmeasinst.2005.11.002

[6] Bignell, N., "The Use of Small Sonic Nozzles at Low Reynolds Numbers," *Flow Measurement and Instrumentation*, Vol. 7, No. 2, June 1996, pp. 109–114. doi:10.1016/S0955-5986(96)00008-8

[7] Choi, Y. M., Park, K. A., Park, J. T., Choi, H. M., and Park, S. O., "Interference Effects of Three Sonic Nozzles of Different Throat Diameters in the Same Meter Tube," *Flow Measurement and Instrumentation*, Vol. 10, No. 3, Sept. 1999, pp. 175–181. doi:10.1016/S0955-5986(98)00050-8

[8] Kim, H. D., Kim, J. H., Park, K. A., Setoguchi, T., and Matsuo, S., "Study of the Effects of Unsteady Downstream Conditions on the Gas Flow Through a Critical Nozzle," *Journal of Mechanical Engineering Science*, Vol. 218, No. 10, Oct. 2004, pp. 1163–1173.

[9] Kim, J. H., Kim, H. D., Park, K. A., Setoguchi, T., and Matsuo, S., "A Fundamental Study of a Variable Critical Nozzle Flow," *Experiments in Fluids*, Vol. 40, No. 1, 2006, pp. 127–134. doi:10.1007/s00348-005-0054-0

[10] Johnson, R. C., "Real-Gas Effects in Critical-Flow-Through Nozzles and Tabulated Thermodynamic Properties," NASA TN D-2565, 1965.

[11] McCarty, R. D., and Weber, L. A., "Thermophysical Properties of Parahydrogen from the Freezing Liquid Line to 5000 R for Pressures to 10,000 Psia," National Bureau of Standards TN 617, April 1972.

[12] Hedere, H., Peter, S., and Wenzei, H., "Calculation of Thermodynamics Properties from a Modified Redlich-Kwong Equation of State," *Chemical Engineering Journal (London)*, Vol. 11, No. 3, 1976, pp. 183–190.

[13] McCarty, R. D., "Hydrogen Technological Survey—Thermophysical Properties," NASA SP 3089, 1975.

[14] Nakao, S., "Development of Critical Nozzle Flow Meter for High Pressure Hydrogen Gas Flow Measurements," Japan Society of Mechanical Engineers Paper G201, 2005.

[15] Soave, G. S., "An Effective Modification of the Benedict–Webb–Rubin Equation of State," *Fluid Phase Equilibria*, Vol. 164, No. 2, Oct. 1999, pp. 157–172. doi:10.1016/S0378-3812(99)00252-6

[16] Yang, J., Griffiths, P. R., and Goodwin, A. R. H., "Comparison of Methods for Calculating Thermodynamic Properties of Binary Mixtures in the Sub and Super Critical State: Lee–Kesler and Cubic Equations of State for Binary Mixtures Containing Either CO_2 or H_2S," *Journal of Chemical Thermodynamics*, Vol. 35, No. 9, Sept. 2003, pp. 1521–1539. doi:10.1016/S0021-9614(03)00129-0

[17] Augnier, R. H., "A Fast Accurate Real Gas Equation of State for Fluid Dynamic Analysis Applications," *Journal of Fluids Engineering*, Vol. 117, No. 2, 1995, pp. 117, 277–281.

[18] Miller, R. W., "Fluid Properties," *Flow Measurement Engineering Handbook*, 3rd ed., McGraw–Hill, New York, 1996, p. 101.

[19] Anderson, J. D., Jr., "Transport Properties in High-Temperature Gases," *Hypersonic and High Temperature Gas Dynamics*, McGraw–Hill, New York, 1998, p. 596.

[20] Nakao, S., Irayama, T., and Takamoto, M., "Relations Between the Discharge Coefficients of the Sonic Venturi Nozzle and a Kind of Gas," *Transactions of the Japan Society of Mechanical Engineers. Series B.*, Vol. 66, No. 642, 2000, pp. 438–444.

J. Oefelein
Associate Editor